

# Robust Charge-based Qubit Encoding

Daniel K. L. Oi,<sup>1,\*</sup> Sonia G. Schirmer,<sup>1</sup> Andrew D. Greentree,<sup>2</sup> and Tom M. Stace<sup>1</sup>

<sup>1</sup>*Department of Applied Mathematics and Theoretical Physics,*

*University of Cambridge, Wilberforce Road, Cambridge CB3 0WA, UK*

<sup>2</sup>*Centre for Quantum Computer Technology, University of Melbourne, Victoria, Australia*

(Dated: November 20, 2018)

We propose a simple encoding of charge-based quantum dot qubits which protects against fluctuating electric fields by charge symmetry of the logical states. We analyze the reduction of coupling to noise due to nearby charge traps and present single qubit gates. The relative advantage of the encoding increases with lower charge trap density.

PACS numbers: 03.67.Lx, 03.65.Yz

## I. INTRODUCTION

Quantum computation faces considerable hurdles, one of the most serious being engineering physical systems performing coherent operations without the deleterious effects of decoherence<sup>1</sup>, particularly in the solid state. However by isolation and manipulation of states of quantum dot (QD) structures<sup>2</sup>, it may be possible to perform many unitary operations within the dephasing time, a pre-requisite for quantum error correction (QEC) by means of Calderbank-Shor-Steane codes<sup>3</sup>.

Underlying logical QEC, a complementary strategy is to use Hilbert subspaces which couple least to noise processes, decoherence free subspaces (DFS)<sup>4,5,6,7</sup>. Practical quantum computing will undoubtedly use elements of both. Charge-based QD quantum computing<sup>8,9,10,11,12,13</sup> is a prime candidate for DFS encoding as electric field coupling is a major source of decoherence<sup>14,15</sup>. Here, we present an architecture incorporating charge symmetry of the logical states to protect against electromagnetic fluctuations, analyze its resistance to charge trap noise and present single-qubit gates. Coupling to charge trap noise and decoherence is suppressed by several orders of magnitude compared to a conventional charge qubit, depending on charge trap density. Alternatives to the passive control implied by DFS encoding include active control sequences, such as Bang-Bang control<sup>16,17</sup>.

In a typical charge-based QD qubit (Fig. 1a) the position of an excess electron defines the logical states. Ideally, the logical states of the system should be eigenstates of the system Hamiltonian when the system is idle, i.e. tunnelling should be suppressed on practical time-scales by  $V_\Omega$ . Furthermore, we assume that the system can be tuned, via  $V_{0,1}$ , such that the logical states are degenerate, hence (known) relative dynamical phases can be neglected.

## II. CLASSICAL NOISE

Fluctuations of the electromagnetic environment superimpose inhomogeneities on the potential seen by the charge states. An electric field component along the axis

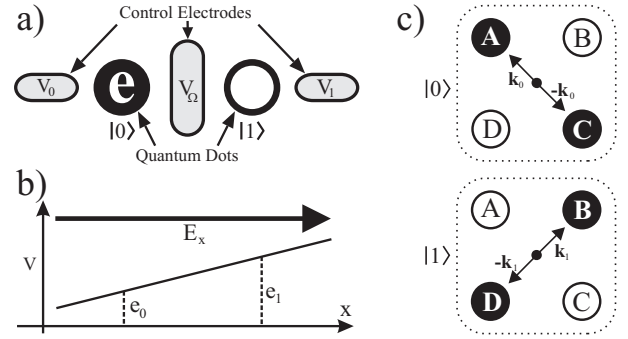


FIG. 1: a) 2QD Dipole Charge Qubit. Logical states,  $\{|0\rangle, |1\rangle\}$ , are defined by an excess electron on the left or right dot respectively. Symmetry electrodes ( $V_{0,1}$ ) control  $\sigma_z$  rotations, and a barrier electrode ( $V_\Omega$ ) controls  $\sigma_x$ . An SET (omitted) measures in the logical basis. b) Temporally and spatially varying potential due to external field. c) 2-Electron 4QD Quadrupole Qubit with  $|0\rangle = a^\dagger c^\dagger |\text{vac}\rangle$ ,  $|1\rangle = b^\dagger d^\dagger |\text{vac}\rangle$ .

of the qubit will cause a sloping potential (Fig. 1b), inducing for each state a different dynamic phase,

$$|j(t)\rangle = e^{-\frac{iq}{\hbar} \int_0^t \epsilon_j(t') dt'} |j(0)\rangle, \quad j = 0, 1 \quad (1)$$

where  $\epsilon_j$  is the on-site energy fluctuation and  $q$  the electron charge. Fluctuations drive superpositions  $|\psi\rangle = \alpha|0\rangle + \beta|1\rangle$  to mixed states,  $|\psi\rangle\langle\psi| \mapsto |\alpha|^2|0\rangle\langle 0| + |\beta|^2|1\rangle\langle 1|$ . Furthermore, electrodes operating on nearby qubits will look like noise, i.e. it may only be practical to actively compensate for operations on nearest neighbors, but not those further away which may also cause unwanted perturbations.

We generalize Eq. (1) to multi-electron configurations, encoding logical states in many-particle states whose geometry protects against decoherence (Fig. 1c)<sup>18,19</sup>. Two excess electrons in diagonally opposite dots define the logical states. Single square QDs in the limit of large dot size should display similar dynamics<sup>20,21</sup>. The 4QD arrangement has also been considered for Coherent Quantum Cellular Automata<sup>22,23</sup>, and for scalable qubits<sup>19</sup>. Measurement in the logical basis can be achieved by a single electron transistor (SET) adjacent to one of the dots in each qubit<sup>14</sup>, or by using multiple SETs in a cor-

related mode<sup>24</sup>. Qutrits or higher dimensional systems may also be considered, e.g. a qutrit encoded as two electrons in a three dimensional 6QD octohedral structure.

An external electric field induces phase shifts, as in Eq. (1), where the energies to first order are

$$\begin{aligned}\epsilon_0(t) &= \epsilon_A + \epsilon_C = 2\bar{V} + \mathbf{k}_0 \cdot \mathbf{E} + (-\mathbf{k}_0) \cdot \mathbf{E} = 2\bar{V} \\ \epsilon_1(t) &= \epsilon_B + \epsilon_D = 2\bar{V} + \mathbf{k}_1 \cdot \mathbf{E} + (-\mathbf{k}_1) \cdot \mathbf{E} = 2\bar{V},\end{aligned}$$

where  $\bar{V}$  is the potential at the common centroid and  $\epsilon_{A,B,C,D}$  are the on-site energy fluctuations of the respective QDs. The symmetrical distributions of charge ensure that each logical state acquires the same dynamic phase due to the external potential gradient. Thus, an initial superposition acquires an *overall* dynamic phase which is unobservable.

### III. CHARGE TRAP NOISE

Though linear spatially varying potentials have no dephasing effect on the 4QD qubit, charge trap fluctuators<sup>24</sup> may pose a problem<sup>25,26,27,28,29</sup>. An occupied charge trap has a  $\sim 1/r$  potential, which perturbs the degeneracy of the DFS states. In principle the charge trap density can be made arbitrarily low but a few charge traps may be unavoidable in practice<sup>39</sup>, and charge trap noise may be a significant source of decoherence.

To understand the effect of charge trap noise, consider a single charge trap coupled to the qubit via the Hamiltonian  $H = k\xi(t)\sigma_z/2$ , where  $\xi = \pm 1$  is a Poisson process of rate  $\lambda$ , and  $k$  is the coupling<sup>30,31</sup>. Averaging over noise processes leads to a decay of the coherence of the qubit density operator,

$$\begin{aligned}\langle \rho_{01}(t) \rangle_\xi &= \rho_{01}(0) \left\langle e^{-ik \int_0^t \xi(t') dt'} \right\rangle_\xi \\ &= \rho_{01}(0) e^{-t\lambda} \left[ \cos \omega t + \frac{\lambda}{\omega} \sin \omega t \right]\end{aligned}$$

where  $\omega = \sqrt{k^2 - \lambda^2}$ . For many independent fluctuators with different rates  $\lambda_j$  and couplings  $k_j$ , the coherence decays in a non-Markovian manner (Fig. 2),

$$\langle \rho_{01}(t) \rangle_\xi = \rho_{01}(0) e^{-t \sum_j \lambda_j} \prod_j \left[ \cos \omega_j t + \frac{\lambda_j}{\omega_j} \sin \omega_j t \right]. \quad (2)$$

A Taylor expansion of the solution (2) about  $t = 0$  shows that the initial decay is parabolic

$$\langle \rho_{01} \rangle_\xi / \rho_{01}(0) \approx 1 - t^2/2 \sum_j k_j^2 + O(t^3), \quad t \ll 1, \quad (3)$$

independent of  $\lambda_j$ , and depends only on the effective coupling of the encoded qubits to the charge traps,  $k_{\text{eff}}^2 = \sum_j k_j^2$  (Fig. 3a). Therefore, the short-term behavior will be dominated by the fluctuator that couples most strongly to the qubit, while the others mainly dampen

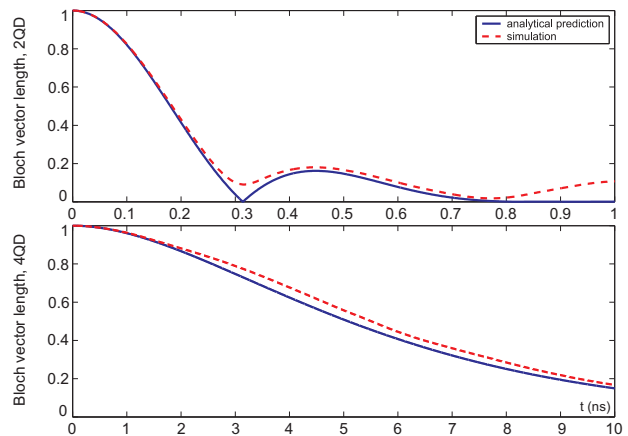


FIG. 2: Qubit Coherence Decay. Initial state  $(|0\rangle + |1\rangle)/\sqrt{2}$  coupled to 100 charge traps.  $k_{\text{eff}}^{(2)} = 12.46 \times 10^9 \hbar/s$  and  $k_{\text{eff}}^{(4)} = 0.60 \times 10^9 \hbar/s$ . A total of 200 quantum trajectories were simulated and averaged. For all simulations, the 2QD qubit was 20nm long and the 4QD qubit was a 20nm square (e.g. P donors in Si, see Ref. 14). Both were located 20nm below the layer in which the charge traps were located. Charge trap transition rate was  $2 \times 10^8 \text{Hz}$ .

further oscillations of the coherence vector (Fig. 2). Furthermore, the time it takes for the coherence to decay from 1 (maximal coherence) to  $p$  for  $p$  close to 1, which is of crucial importance in quantum information processing, is inversely proportional to the effective coupling strength  $k_{\text{eff}}$ ,  $\tau_p = \sqrt{2(1-p)} k_{\text{eff}}^{-1}$ , and we have

$$\frac{\tau_p^{(4)}}{\tau_p^{(2)}} = \frac{k_{\text{eff}}^{(2)}}{k_{\text{eff}}^{(4)}}, \quad (4)$$

where  $k_{\text{eff}}^{(2)}$  and  $k_{\text{eff}}^{(4)}$  is the effective coupling strength for the two-dot and four-dot encoding respectively (Fig. 3 b). Thus, the ratio of the effective coupling strengths is a good measure for the superiority of the 4QD encoding versus the 2QD encoding—the former will be better provided that  $k_{\text{eff}}^{(2)}/k_{\text{eff}}^{(4)} > 1$ , and the larger the ratio the greater the improvement.

The 2QD and 4QD qubits couple differently to charge traps,  $k_j^{(2)} \propto r_j^{-2}$ , and  $k_j^{(4)} \propto r_j^{-3}$  respectively, where  $r_j$  is the distance between the qubit and each charge trap. The 4QD qubit has thus effectively a smaller “horizon” than the 2QD qubit. Hence, generally a charge trap would have to be situated closer to the 4QD qubit than a 2QD qubit to induce the same decoherence. Since the noise on the qubit is generally dominated by the closest fluctuator, whose typical distance is inversely proportional to defect density, the average relative effectiveness of the encoding is therefore expected to increase with decreasing charge trap density, which is confirmed by computer simulations (Fig. 4).

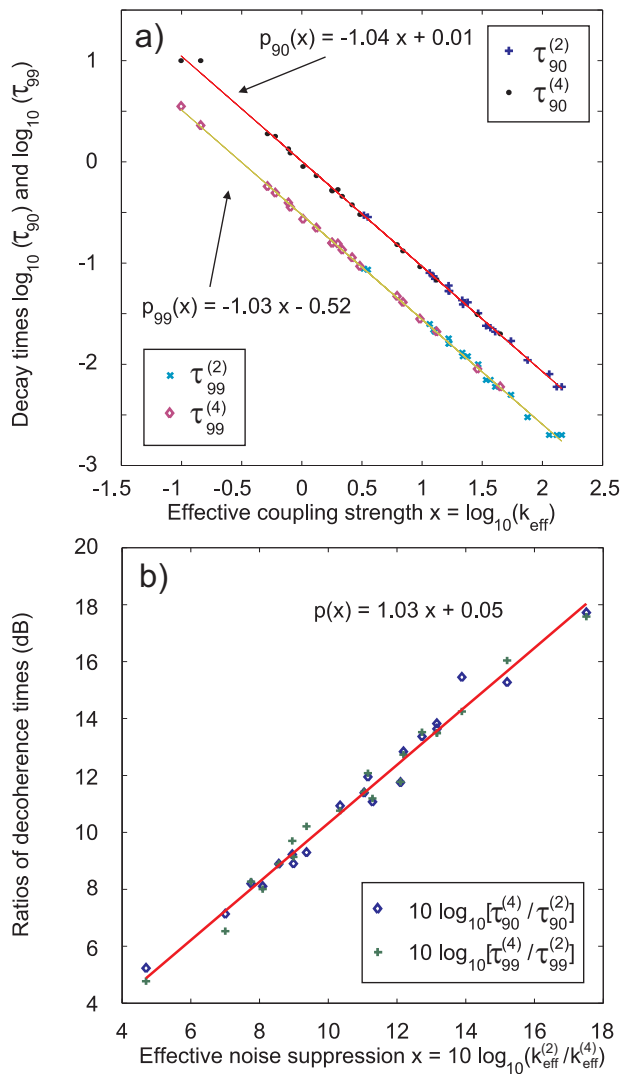


FIG. 3: Decoherence of 2QD and 4QD qubits. (a) The decoherence decay times are inversely related to the effective coupling to fluctuators and show the same dependence for the 2QD and 4QD qubits. (b) The ratio of the short-term coherence times for the 2QD and 4QD encodings are inversely proportional to the ratio of the effective coupling constants. Each point represents the average of 200 quantum trajectories of a qubit coupled to 100 randomly distributed fluctuators.

#### IV. ROBUSTNESS OF ENCODING

The results in the previous section show that the 4QD encoding can substantially increase short-term coherence times for an ideal geometry. However, any physical implementation is likely to deviate from the perfect symmetry of the ideal quantum dot structure. The scheme's sensitivity to such deviations is thus an important practical consideration.

Non-ideal geometry, e.g. due to imperfect QD placement, will introduce a dipole moment, spoiling decoupling from external fields and reducing robustness to charge trap noise. However, as the magnitude of this

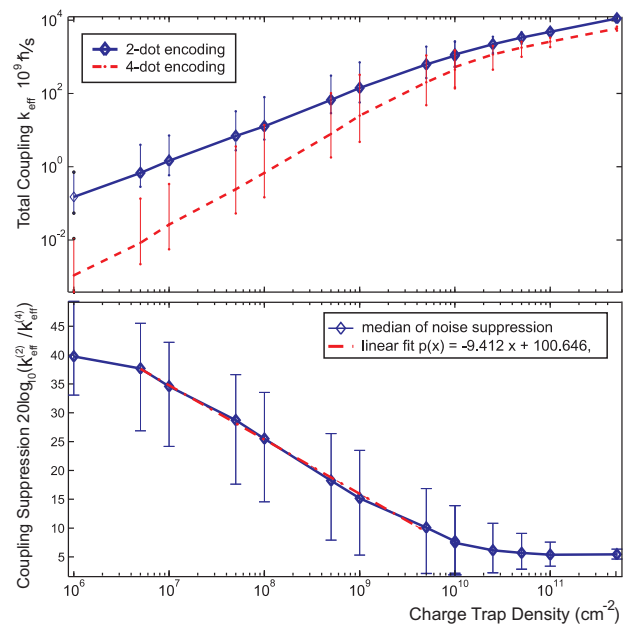


FIG. 4: Coupling and Noise vs Charge Trap Density. Noise suppression of the 4QD vs 2QD qubits was calculated for 100 random charge trap distributions per density, which was then averaged. Coupling strength is in units of  $10^9 \hbar/s$ , bars indicate the 10% – 90% ranges. At high densities, the mean charge trap spacing is comparable to the size of the qubit, leading to saturation effects.

dipole is comparable to, and linear in the displacement, and given that fabrication precision should be at least a fraction of QD spacing for QIP purposes<sup>40</sup>, the extra dipole for the 4QD qubit should be much smaller than for a 2QD qubit, hence the encoding should still offer a noticeable advantage.

To quantify the effect of asymmetry due to placement errors in the quantum dots, we performed extensive simulations computing the effective couplings for various randomly perturbed 2QD and 4QD architectures for different charge trap densities and a wide range of charge distributions. The simulations show that for reasonable errors ( $\sim 10\%$  placement error), the efficiency of the scheme is only modestly affected over a wide range of fluctuator densities (Fig. 5).

#### V. QUANTUM GATES

We now consider implementing a universal set of quantum gates,  $\{\sigma_z^\phi, \sigma_x^{\pi/2}, c - \sigma_z^\pi\}$ . Ideally, we would like all states involved during gate operations to belong to the DFS. This suggests an adiabatic holonomic control scheme<sup>33,34,35</sup>. However, the requirement of additional quantum dots for generating holonomies, charge symmetry constraints on auxiliary dot positioning, and the complexity of pulse sequences all offset possible advantages of holonomic control. Alternatively, rapidly modulating

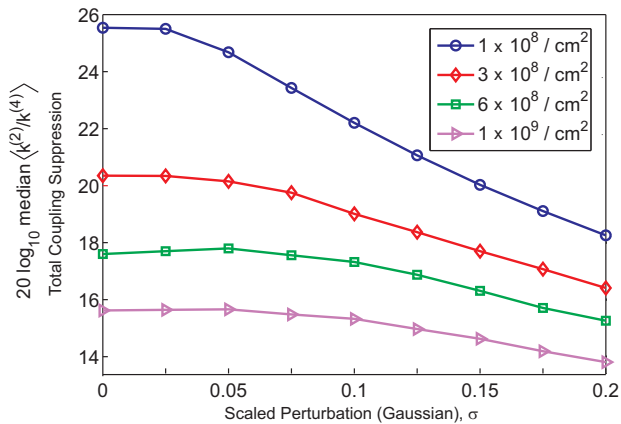


FIG. 5: Decoupling vs Placement Error. We simultaneously and independently perturbed the positions of all quantum dots by a Gaussian displacement with standard deviation  $\sigma$  (expressed as a fraction of the array side-length). This was repeated 1000 times for each of 500 fluctuator distributions. We plot of median w.r.t fluctuator distributions of the mean over the perturbations of the decoupling ratios as a function of error magnitude for different effective fluctuator densities. Even with a 10% displacement error (i.e.  $\sigma = 0.1$ ), the 4QD qubit is still effective.

tunneling between dots can implement the required logical gates quickly. If the gate time is short enough, transient population in non-DFS states, should have minimal coupling to electric field fluctuations. Intra-dot charging should effectively suppress double occupation, which can be further enhanced by ensuring all spins are parallel so that each orbital cannot have more than one electron.

We describe the four dot system as a two-electron, four-site Hubbard model. The electronic creation operators are defined  $a^\dagger, b^\dagger, c^\dagger, d^\dagger$  for dots  $A, B, C, D$  respectively, labelled in clockwise fashion (Fig. 1c). Firstly, the phase gate (a rotation of the Bloch sphere by angle  $\phi$  around the  $z$ -axis)  $\sigma_z^\phi = \text{diag}(1, e^{i\phi})$  is achieved by biasing one pair of diagonally opposite quantum dots with respect to the other,

$$\phi = \frac{2e}{\hbar} \int_0^t [V_0(t') - V_1(t')] dt',$$

where  $V_0, V_1$  are the on-site potentials of the quantum dots defining the  $|0\rangle \equiv a^\dagger c^\dagger |\text{vac}\rangle$  and  $|1\rangle \equiv b^\dagger d^\dagger |\text{vac}\rangle$  states respectively.

Next, the  $\sigma_x^{\pi/2}$  gate requires inter-dot tunnelling. We allow tunnelling between dots  $A \leftrightarrow D$  and  $B \leftrightarrow C$ . Allowing  $A \leftrightarrow B$  and  $C \leftrightarrow D$  tunneling as well leads to similar dynamics but at the expense of extra control electrodes and more non-DFS states involved. With vertical tunneling only, the available state space is spanned by four states,  $\{|0\rangle, |1\rangle, |\varepsilon_0\rangle = a^\dagger b^\dagger |\text{vac}\rangle, |\varepsilon_1\rangle = c^\dagger d^\dagger |\text{vac}\rangle\}$ . Hence the Hamiltonian with no tunneling is,  $H_0^V = \text{diag}(0, 0, \delta, \delta)$  in the above basis, and where we have taken the (degenerate) ground state energy to be 0 and  $\delta$  is the energy of the non-diagonal states  $\{|\varepsilon_0\rangle, |\varepsilon_1\rangle\}$  due to

Coulomb repulsion of the two electrons. We now switch on equal tunneling with rate  $\Omega$  in the vertical direction,

$$H_{\text{tunnel}}^V = \begin{pmatrix} 0 & 0 & \Omega & \Omega \\ 0 & 0 & \Omega & \Omega \\ \Omega & \Omega & 0 & 0 \\ \Omega & \Omega & 0 & 0 \end{pmatrix}.$$

For convenience, we normalize  $\delta = 1$ , and scale  $\Omega$  relative to this. The eigenstates of  $H_{\text{tot}} = H_0 + H_{\text{tunnel}}$  are

$$\begin{aligned} |\psi_1\rangle &= |0\rangle - |1\rangle, \\ |\psi_2\rangle &= |\varepsilon_0\rangle - |\varepsilon_1\rangle, \\ |\psi_3\rangle &= \frac{4\Omega(|0\rangle + |1\rangle)}{\sqrt{1 + 16\Omega^2 + 1}} + |\varepsilon_0\rangle + |\varepsilon_1\rangle, \\ |\psi_4\rangle &= \frac{4\Omega(|0\rangle + |1\rangle)}{\sqrt{1 + 16\Omega^2 - 1}} - |\varepsilon_0\rangle - |\varepsilon_1\rangle, \end{aligned}$$

where the eigen-energies are  $E_1 = 0, E_2 = 1, E_3 = (1 + \sqrt{1 + 16\Omega^2})/2, E_4 = (1 - \sqrt{1 + 16\Omega^2})/2$ . Tunnelling between dots mixes the states so that  $\{|0\rangle, |1\rangle\}$  are no longer eigenstates of  $H_{\text{tot}}$ . Transitions between  $|0\rangle$  and  $|1\rangle$  cannot occur directly but only via transient occupation of the non-DFS states.

In order to achieve a  $\pi/2$  rotation around an axis  $(\cos \gamma, \sin \gamma, 0)$  lying on the equator of the Bloch sphere (which is equivalent to a  $\sigma_x^{\pi/2}$  gate up to  $\sigma_z^\gamma$  rotations)  $|0\rangle \mapsto |0\rangle + e^{i\gamma}|1\rangle, |1\rangle \mapsto |0\rangle - e^{i\gamma}|1\rangle$ , we require  $E_3$  and  $E_4$  to be rational. This leads to the conditions,  $4\Omega = \sqrt{(n/m)^2 - 1}$  where  $\{n/2, m\} \subset \mathbb{Z}^+, n > m$  and  $\text{gcd}(n, m) = 1$ . These requirements derive from the fact that the amplitudes of the  $|0\rangle$  and  $|1\rangle$  should be equal in magnitude when the amplitudes of the non-DFS states are zero, leading to  $jm/n = 1/2 + k, \{j, k\} \subset \mathbb{Z}^+$ , and the gate time  $t_f = 2jm\pi/n$ . When  $t_f = \pi m$ , we achieve the operation with  $\gamma = \pi(n - m)/2$ . If  $t_f = 2\pi m$ , we perform a logical NOT ( $|0\rangle \leftrightarrow |1\rangle$ ).

The minimum gate time for a  $\pi/2$ -gate is  $t_f = \pi$  when  $2 \leq n$  even and  $m = 1$  (Fig. 6). If  $m > 1$ , the time required to implement the gate increases. Coulomb repulsion favors the diagonal charge configurations but transient population in the other states will still occur. For  $n/m \rightarrow 1$ , the gate time is on the order of  $\pi m$  but the maximum transient population scales as  $(n^2 - m^2)/n^2$ . The integrated population in the non-DFS states during the total gate time is proportional to  $m(n^2 - m^2)/n^2$  and thus using smaller tunneling rates does not improve the overall transient occupation of non-DFS states.

The average gate error,  $\mathcal{E} = 1 - \mathcal{F}$  where  $\mathcal{F}$  is the average fidelity<sup>36,37</sup>, for different charge trap couplings (densities) was simulated for 4QD and 2QD qubits. The ratio of the errors, presented in Fig. 7, show that despite transient population in non-DFS states during the operation of the  $\sigma_x^{\pi/2}$ -gate, the 4QD configuration still shows a significant advantage over the 2QD qubit.

A universal two-qubit controlled-phase ( $c-\phi$ ) gate may be implemented as suggested in earlier work<sup>38</sup>. A transient deformation of the charge distribution of adjacent

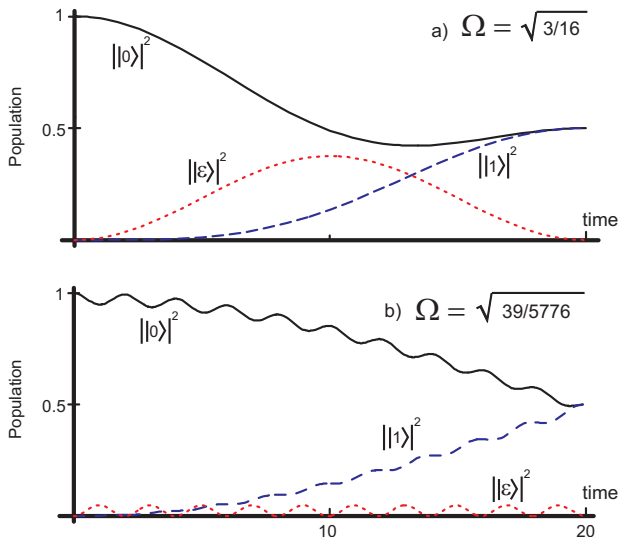


FIG. 6: Populations During  $\sigma_x^{\pi/2}$ -Gate vertical tunneling. An initial state  $|0\rangle$  is transformed into  $(|0\rangle + i|1\rangle)/\sqrt{2}$  with transient population in non-DFS subspace  $|\epsilon\rangle$ . a)  $\Omega$  large:  $n = 2$ ,  $m = 1$ , b)  $\Omega$  small:  $n = 20$ ,  $m = 19$ .

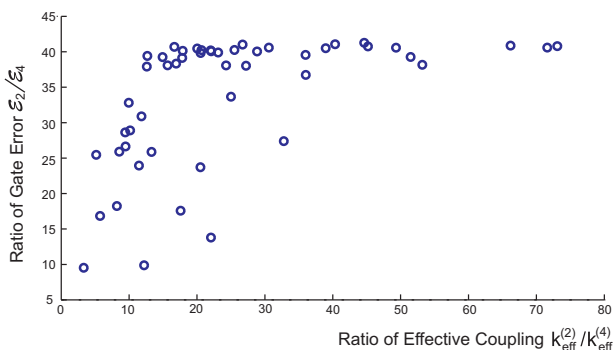


FIG. 7:  $\sigma_x^{\pi/2}$ -Gate Error vs Noise Coupling. Gate parameters:  $t_f \approx 50\text{ps}$ ,  $\Omega_2 = \pi/(4t_f)$ ,  $\delta = 3.84 \times 10^{12}\text{h/s}$ ,  $4\Omega_4 = \delta_c \sqrt{(62/61)^2 - 1}$ . Fidelity was calculated from 50 trajectories per initial state  $\{| \pm x \rangle, | \pm y \rangle, | \pm z \rangle\}$ .

qubits by the use of auxiliary quantum dots would allow modulation of an effective  $\sigma_z \otimes \sigma_z$  interaction. Charge symmetry could still be maintained during the gate by use of auxiliary dots.

## VI. CONCLUSION

We have analyzed the noise suppression of a 2-electron 4QD qubit encoding, which decouples from linearly varying fields. For nearby charge fluctuators, the decoupling depends upon the exact distribution, but analytic and numerical results show considerable enhancement of noise resistance and coherence times, increasing at low charge trap densities. This advantage persists in the presence of dot placement errors. We show how to construct single qubit rotations, and two-qubit gates may be possible via previously proposed schemes for conventional charge qubits. Characterization and tuning of the 4QD qubit should be similar to that for a conventional 2QD qubit. The architecture requires only a modest increase in complexity and may also be applied to systems such as super-conducting charge qubits.

## Acknowledgments

SGS, DKLO and TMS acknowledge Fujitsu, Cambridge-MIT Institute, EPSRC (UK), and EU grants RESQ (IST-2001-37559) and TOPQIP (IST-2001-39215). DKLO is supported by Sidney Sussex College Cambridge. ADG is supported by the Australian Research Council, the Australian government, and NSA, ARDA and ARO under DAAD19-01-1-0653. ADG acknowledges the generosity of Fujitsu whilst visiting Cambridge. We are grateful to Christina Goldschmidt for useful discussions.

\* Electronic address: D.K.L.Oi@damtp.cam.ac.uk  
<sup>1</sup> W. H. Zurek, *Physics Today* **44**, 36 (1991).  
<sup>2</sup> D. P. DiVincenzo, D. Bacon, J. Kempe, G. Burkard and K. B. Whaley, *Nature* **408**, 339 (2000).  
<sup>3</sup> A. M. Steane, *Phys. Rev. Lett.* **77**, 793 (1996).  
<sup>4</sup> P. Zanardi and M. Rasetti, *Phys. Rev. Lett.* **79**, 3306 (1997).  
<sup>5</sup> D. A. Lidar, I. L. Chuang and K. B. Whaley, *Phys. Rev. Lett.* **81**, 2594 (1998).  
<sup>6</sup> P. Zanardi and F. Rossi, *Phys. Rev. Lett.* **81**, 4752 (1998).  
<sup>7</sup> M.V. Feigel'man, L.B. Ioffe, V.B. Geshkenbein, P. Dayal and G. Blatter, *Phys. Rev. B* **70**, 224524 (2004).  
<sup>8</sup> A. Ekert and R. Jozsa, *Rev. Mod. Phys.* **68**, 733 (1996).  
<sup>9</sup> T. Hayashi, T. Fujisawa, H. D. Cheong, Y. H. Jeong and Y. Hirayama, *Phys. Rev. Lett.* **91**, 226804 (2003).  
<sup>10</sup> S. G. Schirmer, A. D. Greentree and D. K. L. Oi,

arXiv:quant-ph/0305052 (2003).  
<sup>11</sup> J. R. Petta, A. C. Johnson, C. M. Marcus, M. P. Hanson, and A. C. Gossard, *Phys. Rev. Lett.* **93**, 186802 (2004).  
<sup>12</sup> J. Gorman, D. G. Hasko, and D. A. Williams, arXiv:cond-mat/0504451 (2005).  
<sup>13</sup> T. M. Buehler, V. Chan, A. J. Ferguson, A. S. Dzurak, F. E. Hudson, D. J. Reilly, A. R. Hamilton, R. G. Clark, D. N. Jamieson, C. Yang, C. I. Pakes and S. Praver, arXiv:cond-mat/0506594 (2005).  
<sup>14</sup> L. C. L. Hollenberg, A. S. Dzurak, C. Wellard, A. R. Hamilton, D. J. Reilly, G. J. Milburn and R. G. Clark, *Phys. Rev. B* **69**, 113301 (2004).  
<sup>15</sup> S. D. Barrett and G. J. Milburn, *Phys. Rev. B* **68**, 155307 (2003).  
<sup>16</sup> L. Viola and S. Lloyd, *Phys. Rev. A* **58**, 2733 (1998).  
<sup>17</sup> E. Fraval, M. J. Sellars, and J. J. Longdell,

- arXiv:quant-ph/0412061 (2004).
- <sup>18</sup> G. Tóth, A. O. Orlov, I. Amlani, C. S. Lent, G. H. Bernstein and G. L. Snider, *Phys. Rev. B* **60**, 16906 (1999).
- <sup>19</sup> G. Tóth and C. S. Lent, *Phys. Rev. A* **63**, 052315 (2001).
- <sup>20</sup> C. E. Creffield and G. Platero, *Phys. Rev. B* **66**, 235303 (2002).
- <sup>21</sup> J. H. Jefferson, M. Fearn, D. L. J. Tipton and T. P. Spiller, *Phys. Rev. A* **66**, 042328 (2002).
- <sup>22</sup> J. H. Cole, A. D. Greentree, C. J. Wellard, L. C. L. Hollenberg and S. Praver, *Phys. Rev. B* **71**, 115302 (2005).
- <sup>23</sup> S. Gardelis, C. G. Smith, J. Cooper, D. A. Ritchie, E. H. Linfield and Y. Jin, *Phys. Rev. B* **67**, 033302 (2003).
- <sup>24</sup> T. M. Buehler, D. J. Reilly, R. Brenner, A. R. Hamilton, A. S. Dzurak and R. G. Clark, *Appl. Phys. Lett.* **82**, 577 (2003).
- <sup>25</sup> T. Itakura and Y. Tokura, *Phys. Rev. B* **67**, 195320 (2003).
- <sup>26</sup> M. Schultz, *Surf. Sci.* **132** 422 (1983).
- <sup>27</sup> H. H. Mueller and M. Schultz, *J. Appl. Phys.* **83**, 1734 (1998).
- <sup>28</sup> D. R. McCamey, M. Francis, J. C. McCallum, A. R. Hamilton, A. D. Greentree and R. G. Clark, *Semicond. Sci. Tech.* **20**, 363 (2005).
- <sup>29</sup> J. C. Ang, C. J. Wellard, L. C. L. Hollenberg, *Proc. of SPIE* **5650**, 527 (2005).
- <sup>30</sup> Y. M. Galperin, B. L. Altshuler and D. V. Shantsev, *Proc. Conf. Fund. Prob. of Mesoscopic Phys: Interactions & Decoherence*, Spain (2003) arXiv:cont-mat/0312490 (2003).
- <sup>31</sup> F. Meier and D. Loss, *Phys. Rev. B* **71**, 094519 (2005).
- <sup>32</sup> S. R. Schofield, N. J. Curson, M. Y. Simmons, F. J. Rueß, T. Hallam, L. Oberbeck and R.G. Clark, *Phys. Rev. Lett.* **91**, 136104 (2003)
- <sup>33</sup> P. Zanardi and M. Rasetti, *Phys. Lett. A* **264**, 94 (1999).
- <sup>34</sup> R. G. Unanyan, B. W. Shore and K. Bergmann, *Phys. Rev. A* **59**, 2910 (1999).
- <sup>35</sup> L.-M. Duan, J. I. Cirac and P. Zoller, *Science* **292**, 1695 (2001).
- <sup>36</sup> J. F. Poyatos, J. I. Cirac and P. Zoller, *Phys. Rev. Lett.* **78**, 390 (1997).
- <sup>37</sup> M. D. Bowdrey, D. K. L. Oi, A. J. Short, K. Banaszek and J. A. Jones, *Phys. Lett. A* **294**, 258 (2002).
- <sup>38</sup> S. G. Schirmer, D. K. L. Oi and A. D. Greentree, *Phys. Rev. A* **71**, 012325 (2005)
- <sup>39</sup> For thick SiO<sub>2</sub> layers on Si, defect densities of  $\sim 10^8 \text{cm}^{-2}$  have been achieved<sup>26</sup>. Trap densities for thin oxide layers of order  $\sim 10^{11} \text{cm}^{-2}$  have been reported in Refs. 27,28
- <sup>40</sup> Atomic-scale placement ( $\sim 1 \text{ nm}$  accuracy) of P donors in Si has been demonstrated<sup>32</sup>.